I&EC research
Industrial & Engineering Chemistry Research

ARTICLE

pubs.acs.org/IECR

Surfactant-Enhanced Multiscale Carbon Webs Including Nanofibers and Ni-Nanoparticles for the Removal of Gaseous Persistent Organic Pollutants

Mekala Bikshapathi,[†] Gyanesh N. Mathur,[†] Ashutosh Sharma,[*,†,‡] and Nishith Verma[*,†,§]

[†]Department of Chemical Engineering, [‡]DST Unit on Nanosciences, and [§]Center for Environmental Science and Engineering, Indian Institute of Technology Kanpur, Kanpur-208016, India

ABSTRACT: Nickel (Ni) impregnated activated carbon fibers (ACFs) were used as a substrate to grow carbon nanofibers (CNFs) for the removal of persistent gaseous organic pollutants. A surfactant (cetyl trimethylammonium bromide) was used in the impregnating solution of nickel nitrate hexahydrate, which helps to create much smaller and denser Ni particle (catalyst) distribution on ACF for CNF-growth. Temperature programmed reduction, atomic absorption spectroscopy, X-ray diffraction spectroscopy, and adsorption tests were used to characterize and compare the products. Scanning electron microscopy and H_2-chemisorption were used to investigate the surface morphology and the active metal sites, respectively, of the prepared adsorbent. The adsorption performance of ACF/CNF evaluated under flow conditions established that the adsorption of the gaseous pollutant was larger on the CNFs prepared using the surfactant than on the CNFs grown without using the surfactant.

INTRODUCTION

Persistent organic pollutants (POPs) are chemical compounds that persist in the environment for relatively long period and are gradually accumulated in the biosystem. POPs such as dieldrin, aldrin, an endrin, pose risk to the human health and the ecosystem, if present even at very low concentrations. Though most of the research activities are on the identification and analysis of POPs, little work has been reported on the removal or control of POPs.[1−5] Therefore presently there is an increasing need for effective and efficient methods to control POPs.

Adsorption is considered to be an energy and cost-effective method to control the gaseous as well as aqueous phase pollutants, especially if the concentration levels of the pollutants are low (ca. ppm or subppm). Literature is replete with studies on granular activated carbons (GACs) or powdered activated carbons (PACs) for the environmental remediation applications. Activated carbon fibers (ACFs) are relatively new materials as adsorbents.[6−10]

More recently, the multiscale carbon web including carbon nanofibers (CNFs) was developed and used for the efficient removal of NO from air, and fluoride, arsenic, and lead ions from water.[11−15] The multiscale or hierarchal carbon web was developed by growing CNFs on ACFs by catalytic chemical vapor deposition (CCVD). The advantage of such a multiscale carbon web is that the prepared web may be directly used in an end-application without requiring the postsynthesis step for subsequently removing and/or transferring the web to another porous substrate for use. In addition, the prepared web has a large surface area for adsorption.

Agglomeration of the metal catalytic particles during the ACF-impregnation step is the major hindrance to the development of the efficient carbon micronano-hierarchal web. The agglomeration of the metal particles in the impregnating solution results in the transfer of relative large-size metal-particles to the ACF-surface, which in turn causes blockage of pores in ACF, ultimately leading to sparse and less growth of CNFs during the CCVD step. The adsorbents thus prepared are less efficient. The present study describes the preparation of ACF/CNF composites using a surfactant during the metal-impregnation step with a view to overcome the agglomeration of the metal catalytic particles.

The utility and role of surfactants in preparing metal nanoparticles are well recognized. There have been several studies on the synthesis of metal nanoparticles using different surfactants for stabilizing uniform-sized particles in solutions.[16−26] Surfactants have also been successfully used for dispersing carbon nanotubes (CNTs) in the liquid-phase.[27,28] Surfactants promote the stable dispersion of particles in solution by accretion at their surface. Surfactant adsorption reduces the particle interfacial tension and thus prevents particles from aggregating in the solution by introducing a net repulsion. The adsorbed layer also "caps" or retards the further growth of nanoparticles. These factors allow a stable dispersion of relative small sized nanoparticles in the solution.[29,30]

Metal nanoparticles have been synthesized in aqueous and organic solutions, using various surfactants, such as cetyl trimethylammonium bromide (CTAB), tri-n-octylphosphine oxide (TOPO), and sodium dodecyl sulfate (SDS). In general, it is difficult to prepare nanoparticles of metals in solutions because the particles tend to convert into metal oxides, or other forms, due to their high reactivity. In this study, micrometer-size ACFs were, therefore, first dispersed with salts of nickel nitrate hexahydrate using CTAB in an impregnating solution of acetone. The salts dispersed in ACF were then converted in situ to the

Special Issue: Nigam Issue

Received: April 7, 2011
Accepted: July 11, 2011
Revised: July 1, 2011
Published: July 11, 2011

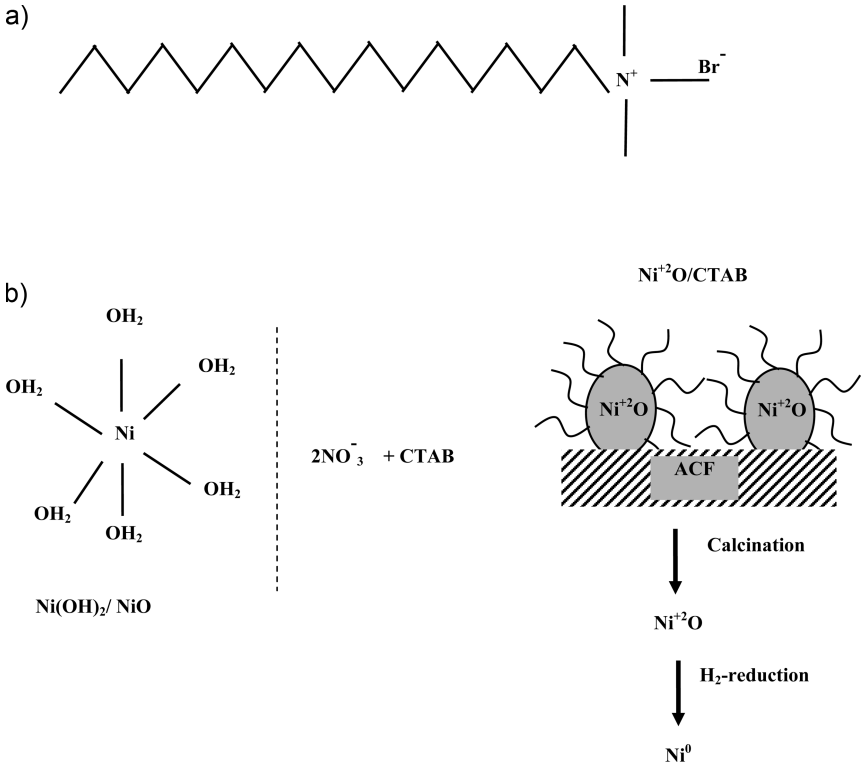

Figure 1. (a) Chemical structure of CTAB. (b) Transfer of Ni-salts from the impregnating solution to the ACF-surface, using CTAB, and the subsequent fate of Ni-salts on ACF.

metallic state (Ni^0) by calcination, followed by reduction in a H_2-atmosphere. The resulting Ni-ACF was subsequently used as a substrate to grow CNFs by CCVD.

The prepared hierarchal web of carbon microfibers and nanofibers (ACF/CNF) was applied as an adsorbent for the removal of POPs. For this adsorption study, 2-chloroethanol was chosen as the model organic pollutant. 2-Chloroethanol is also classified as a category-2 chemical warfare agent, which is known to be highly toxic to humans, as well as to the ecosystem.[10] The characterization of the new adsorbent confirmed highly improved performance compared to the conventional way of making ACF/CNF adsorbents.

MATERIALS AND METHODS

CTAB and CNF-Growth on ACF. Figure 1a describes the chemical structure of the CTAB surfactant molecule employed in this study for the preparation of Ni catalyst impregnated multiscale carbon webs. The head of the molecule contains the positively charged quaternary ammonium cation. When CTAB is added to the impregnating solution of nickel nitrate hexahydrate, the CTAB molecule attaches to the surface of Ni-particles, which prevents the neighboring particles from agglomeration. Therefore, particle segregation is achieved in the bulk liquid solution. The segregation results in a reduction of particle size. Subsequently, an increasingly large amount of nickel is transferred to the ACF surface, along with CTAB. During the calcination step, CTAB decomposes leaving behind NiO particles, with further reduction achieved in the particle size. Subsequently, when NiO-ACF is reduced in H_2 atmosphere, the NiO particles are converted into their pure metallic (Ni^0) state. Figure 1b contains the schematic description of the transfer of Ni salts from the impregnating solution to the ACF surface and the subsequent processing of the Ni-salts on ACF, as discussed above.

Figure 2 is the schematic illustration of the various steps associated with the preparation of CNF on Ni-ACF. The primary steps are the impregnation of ACF with Ni-salts using CTAB in acetone, calcination at high temperature, and reduction in the H_2 atmosphere. During CCVD, the decomposition of C_6H_6 occurs on the active Ni particles, with the dissolution of carbon and its diffusion through the Ni particle. CNFs subsequently grow by the tip-growth mechanism. In such cases, the precipitation of carbon occurs at the rear face of the Ni particle in the form of a hexagonal graphite platelet.[31−33]

Reagents. AR grade nickel nitrate hexahydrate (>97%) [$Ni(NO_3)_2.6H_2O$], 2-chloroethanol (>99%), acetone, and the GR grade *N*-Cetyl-*N*,*N*,*N*-trimethyl ammonium bromide (CTAB) were purchased from Merck (Germany). Nitrogen (>99%), hydrogen (>99%), and zero air (>99%) were obtained from Sigma Gases (India). The phenolic resin precursor-based ACF was purchased from Kynol Inc. Tokyo (Japan).

Preparation of $Ni(NO_3)_2$ Dispersed ACFs. The Ni-ACFs were prepared using $Ni(NO_3)_2 \cdot 6H_2O$ as the Ni precursor and CTAB as a surfactant in acetone by the incipient wetness impregnation method. Different CTAB-concentrations (1%, 3%, 5%, 7%, and 10%, all w/w) were used to impregnate different ACF samples. In this study, ACF/CNFs are used to represent the ACF/CNF composite grown using *n*% CTAB-concentrations.

The ACF samples were first pretreated in deionized (DI) water at 80 °C for 6 h to leach out any undesirable ions and increase the affinity of the ACF surface to the metals during the impregnation step. The wet ACF samples were then dried for 4 h in still-air at room temperature (35 ± 2 °C) and were subsequently oven-dried at ∼120 °C. Next, an approximately 1 g sample of the oven-dried

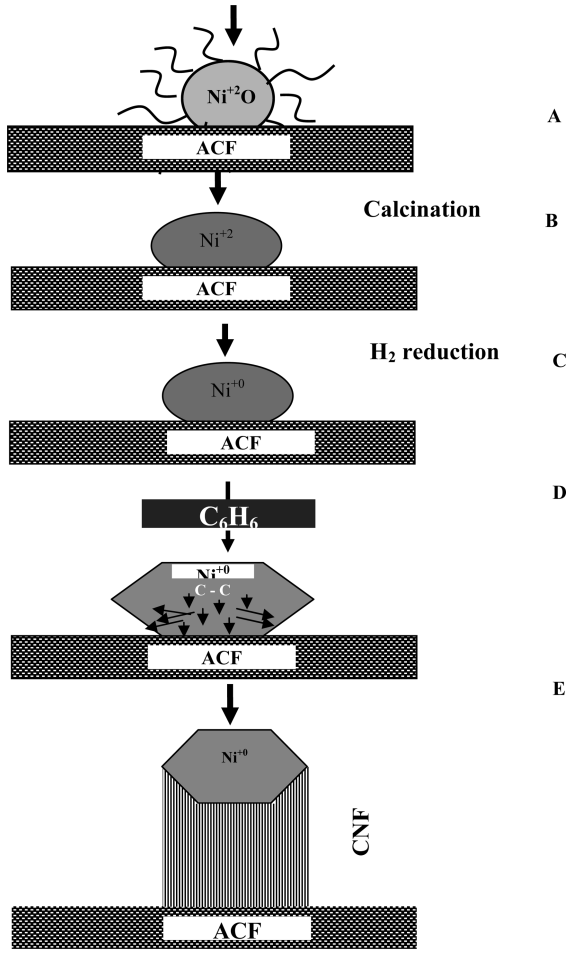

Figure 2. Schematic illustration of the various steps associated with the preparation of CNFs on ACF. (A) Impregnation of ACF with Ni-salts using CTAB in acetone, (B) calcinations at high temperatures, (C) reduction in H_2 atmosphere, (D) decomposition of C_6H_6 on the active Ni-particles, with the dissolution and diffusion of carbon through the Ni-particle, and (E) growth of CNF by the tip-growth mechanism.

ACF was wrapped over a perforated glass tubular reactor for vacuum drying at 200 °C for 12 h to remove any entrapped gases from the pores of ACF. The vacuum-dried ACF was quickly connected to a round bottomed flask containing 0.4 M impregnating solution of $Ni(NO_3)_2 \cdot 6H_2O$ in acetone. The solution also contained CTAB, which was added to the solution of Ni-salts and acetone and mixed for 30 min using a magnetic stirrer, before starting the impregnation. The impregnating solution of the ACF sample was recycled through the ACF sample for 6 h using a peristaltic pump. Some $Ni(NO_3)_2$-ACFs samples were also prepared without using surfactant.

Preparation of CNFs. CNFs were prepared by CCVD in a horizontal tubular reactor, shown in Figure 3. The horizontal reactor was constructed of a stainless steel (SS) tube, 30 mm in diameter and 1000 mm in length. The reactor was installed in a horizontal electric furnace with provisions made for the gas inlet and outlet. The same horizontal reactor was also used for calcinations and H_2-reduction of the salts contained in the ACF samples impregnated with nickel salt.

The $Ni(NO_3)_2$-ACFs samples that were prepared in the previous (impregnation) step were calcined at 400 °C for 4 h under a small N_2-flow at 0.1 standard liter per min (slpm) and were

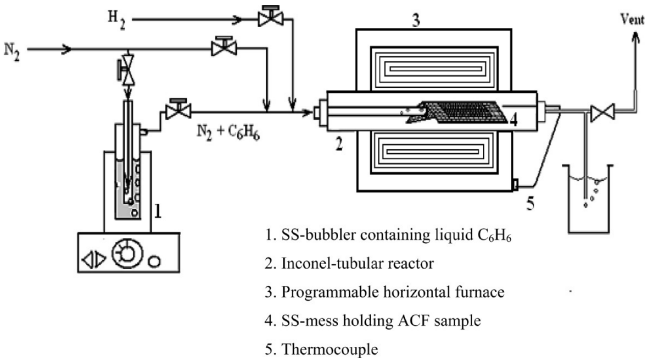

Figure 3. Schematic diagram of the experimental setup used for the growth of CNFs.

Table 1. AAS Data: The Loading of Ni in Different Impregnated ACF Samples

sample	C_{CTAB} (%)	loading (g/g)
0.4 M, $Ni+^2$—ACF	0	0.23
	1	0.29
	3	0.39
	5	0.63
	7	0.31
	10	0.28

subsequently reduced at 500 °C for 2 h under H_2 atmosphere at a flow-rate of 0.15 slpm. The above calcinations and reduction temperatures were optimized based on the TPR profiles; this optimization is discussed later in the manuscript. To grow the CNF on the Ni-ACF, a Freon-refrigerator and a SS tubular gas bubbler were used to vaporize the hydrocarbon (C_6H_6) feed stock solution. The temperature of the refrigerator was constantly maintained at 5 °C. N_2 was used as a carrier gas and flowed at the rate of 0.2 slpm into the SS bubbler containing the C_6H_6. Next, the mixture of N_2 saturated with C_6H_6 was introduced into the reactor. CCVD was carried out for 1 h at 800 °C. After CCVD, the reactor was slowly cooled to room temperature (25 ± 5 °C) under N_2 flow at 0.1 slpm.

RESULTS AND DISCUSSION

Surface Characterization. *Atomic Absorption Spectroscopy (AAS).* AAS (model: AA240, Varian, Australia) analysis was carried out to determine the metal (Ni) loading in the ACF samples following impregnation with and without using CTAB. Table 1 presents the data of Ni-loading (g/g) in the Ni-impregnated ACF samples. As observed, the loading varied from 0.23 g/g to 0.63 g/g and the CTAB concentration varied from 0 to 10%. The amount of Ni in ACF increased with increasing CTAB concentration up to 5% concentration. Beyond 5% CTAB concentration, the amount of Ni-transferred from the bulk impregnating solution to the ACF-surface actually decreased. At a 10% CTAB concentration, the metal loading drastically decreased to 0.28 g/g. This may be because at relatively higher CTAB concentrations, excess CTAB can form micelles, get adsorbed on ACF and also form barriers around Ni-particles. All of these could possibly reduce the attachment of the particles from the bulk solution to the surface of the ACF. On the basis of the data described above, all Ni-ACF samples used to grow CNFs

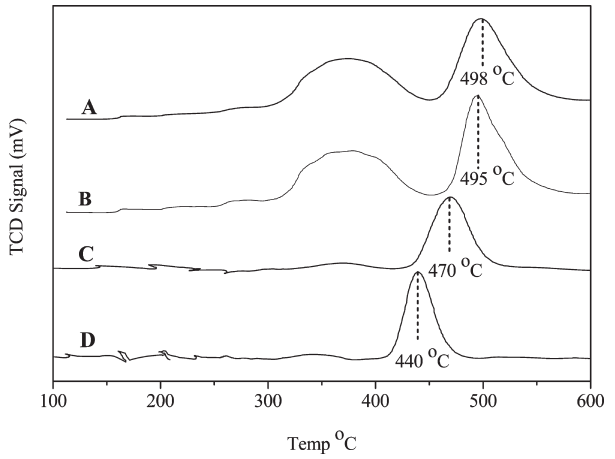

Figure 4. TPR profiles of the NiO-ACF samples prepared at different calcination temperatures (A) 450, (B) 400, (C) 350, and (D) 300 °C to determine the optimum reduction temperature.

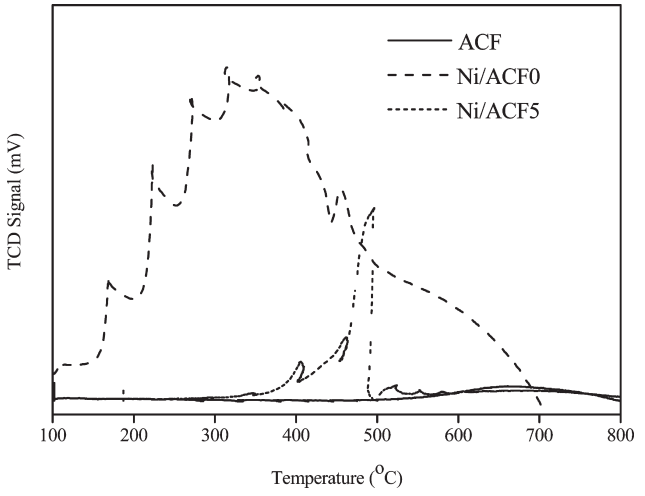

Figure 5. TPR profiles of ACF and ACF/CNF samples prepared with and without using CTAB.

in this study were prepared at an optimal 5% CTAB concentration. In summary, the nickel-loading was largest on the ACF surface when the optimal concentration of CTAB was used.

Temperature-Programmed Reduction (TPR). H_2-TPR analysis was carried out to determine the optimum calcinations and reduction temperatures for Ni-impregnated ACF samples, and also to ascertain the reducibility of NiO in the presence of CTAB. A Quantachrome Instrument (model: Autosorb 1C), fitted with a thermal conductivity detector (TCD), was used for TPR analysis. The analysis was carried out using a mixture of 5% H_2-N_2 as the reducing agent. The samples were first degassed at 200 °C for 4 h under a helium atmosphere and were then purged with a 5% H_2-N_2 mixture for 30 min at 40 °C to clean the surface. The samples were then heated at a rate of 10 K min^{-1} to 1073 K under the reducing agent. The initial TCD signal was set at 0 mV using coarse and fine knobs and the TCD current was set at 150 mA.

Figure 4 presents the TPR profiles of different NiO-ACF samples obtained following calcinations at different temperatures (300, 350, 400, and 450 °C) of the Ni-salt impregnated ACFs.

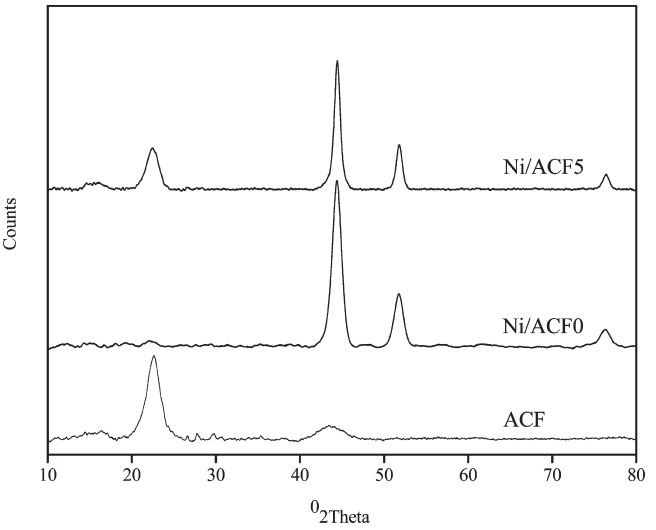

Figure 6. XRD patterns of ACF and Ni-ACFs prepared with and without using CTAB.

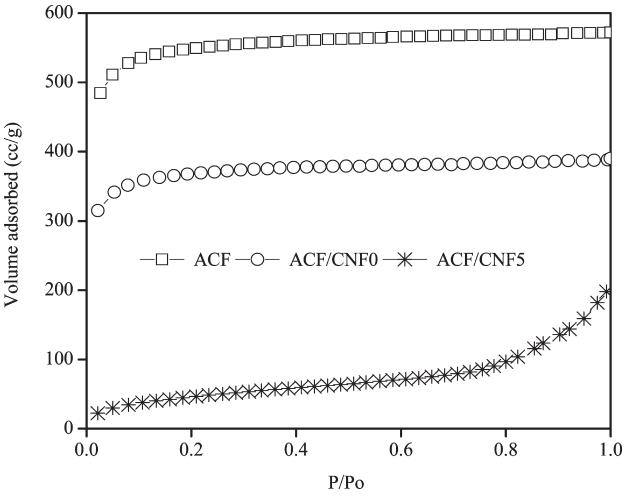

Figure 7. N_2 adsorption isotherms of ACF and ACF/CNF samples at 77 K.

The calcination time was 4 h for all the samples. A reduction peak was obtained at 440 °C for the NiO-ACF sample calcined at 300 °C (Figure 4). However, the peak shifted to higher temperatures, 470, 495, and 498 °C for the samples calcined at 350, 400, and 450 °C, respectively. No appreciable shift was observed for the samples calcined at higher temperatures (>400 °C). This suggests that all Ni-nitrate particles were completely converted into NiO at around 400 °C. Based on these data, the calcination and reduction temperatures were set to 400 and 500 °C, respectively, for the production of CNFs.

Figure 5 compares the TPR profiles for Ni-ACF5 to those for Ni-ACF0 and ACF. As expected, the ACF sample did not produce reduction-peaks within the temperature range tested for the TPR profiles. However, several dominant reduction peaks were observed over the temperature range of 150−350 °C and one major peak was observed at 450 °C, for the Ni-impregnated samples (Ni-ACF0) prepared without using CTAB. This peak is attributed to the presence of NiO-crystals in the ACF, which

Table 2. Surface Area, Total Pore Volume, and PSD Data[a]

sample	C_{CTAB} (w/w%)	S_{BET} (w/w%)	V_t (cc/g)	PSD micro	PSD meso	PSD macro	D_{avg} (nm)
ACF		1567	0.887	87.91	7.10	4.99	2.265
ACF/CNF0	0	1035	0.588	85.88	10.09	4.03	2.272
ACF/CNF5	5	232	0.334	28.91	65.45	5.65	5.754

[a] Abbreviations: C_{CTAB} = concentration of CTAB (w/w %), S_{BET} = specific surface area based BET method, V_t = total pore volume, D_{avg} = average pore diameter.

were relatively large and may not have been prone to complete H_2-reduction. The observed reduction profile for the Ni-ACF5 samples was different in the following respects: (1) there was only one dominant peak, and (2) the corresponding reduction temperature was ~495 °C. The relative higher temperature observed for Ni-ACF5 may be attributed to the large energy required for the complete reduction. As earlier mentioned in the manuscript, the metals loading on Ni-ACF5 prepared using the optimized concentration of CTAB was significantly larger than on Ni-ACF0. In such a case, a relatively larger number of small crystals were produced, which were dispersed mostly within the micropores of Ni-ACF.

X-ray Diffraction Spectrocopy (XRD). The XRD patterns of the ACF-Ni samples, prepared with and without surfactants, were recorded on an X-pert X-ray diffractometer, with Cu Ka (k = 1.54178 A°) over the 2θ-range of 10°−80° at a step size of 0.01. For comparison, the XRD spectra of the ACF samples (as received, prior to any treatment) were also recorded and are shown in Figure 6.

No Ni-peaks were observed in the as-received ACF samples. However, three characteristic peaks were observed for Ni particles at 2θ of 44.5°, 51.8°, and 76.5°, which correspond to the crystallographic indices of (111), (200), and (222) planes, respectively. The spectra also revealed that the prepared samples contained Ni in its pure metallic FCC phase. Additionally, a common peak was observed around 22° (2θ) in all the samples, which is characteristic of amorphous carbon with crystallographic indices of 002. The intensities of the Ni-peaks at 44.5, 51.8, and 76.5 (°2θ) were observed to be increased for the Ni-ACF5 sample compared to the Ni-ACF0 sample.

The sizes of the Ni-particles in the Ni-ACF0 samples were calculated using Scherrer's formula and were found to be 14 nm. The size drastically decreased to 6 nm for Ni-ACF5. Therefore, we infer that the surfactant helped to control the size of the Ni-particles by the monodispersion of Ni on the ACF surfaces and that the surfactant facilitated maximum transfer of Ni from the bulk impregnating solution to the ACF surface, with minimum pore blockage. This was corroborated in the previous discussion of the AAS data. Therefore, it can be concluded from the analysis of the XRD data that small sized nickel particles were produced using CTAB. This helped in producing dense CNFs of small diameter, as described later.

Surface Area and Pore Size Distribution. The N_2 adsorption−desorption isotherms were obtained at 77 K at relative pressures (P/P_o) from 0 to 1, using the Quantachrome Autosorb Instrument (model: Autosorb 1C). Prior to analysis, approximately 40 mg of the ACF sample was loaded into the sample-cell and was degassed for 8 h at 200 °C under vacuum (10 μm Hg). The sample was cooled to room temperature (30 ± 2 °C) and subjected to adsorption−desorption analysis. The total specific surface area (S_{BET}) of the samples was determined by applying the Brenner−Emmett−Teller (BET) equation to the isotherm data over a P/P_o range of 0.05−0.35. The BET eq ($1/V(P/P_o - 1)$ *vs* P/P_o) is usually linear over this range of relative pressures (P/P_o).[34] The amount of N_2 gas adsorbed at a relative pressure near unity (~0.9994) was used to calculate the total pore volume (V_t). For the analysis of meso- and micropore volumes, the Barrett−Joyner−Halenda (BJH) and density functional theory (DFT) methods were applied over pore sizes ranging from 2−40 nm and ≤2 nm, respectively, of the desorption isotherms by assuming slit-type pores in ACF.

Table 3. Chemisorption Data[a]

sample	concentration of CTAB (%)	ASA (m^2/g of sample)	metal dispersion (%)
Ni-ACF	0	0.351	1.31
	5	0.713	2.67

[a] Abbreviations: C_{CTAB} = concentration of CTAB, ASA = active metal surface area.

The adsorption isotherms for ACF and ACF/CNF samples are shown in Figure 7. For the ACF sample, the volume of adsorbed gas (N_2) steeply increased below $P/P_o \approx 0.01$ before gradually leveling off. The isotherms of ACFs are type I, which shows that the materials are microporous. For ACF/CNF samples, a steep increase in the adsorbed volume was again observed beyond $P/P_o \approx 0.9$. This is a common characteristic of N_2-adsorption isotherms and is observed in most of nanostructured materials.[35,36] The ACF/CNF5 composites exhibit type II isotherms, which are commonly observed in microporous materials having narrow pores, which are not accessible to N_2.

Table 2 presents the data obtained by the N_2-physisorption analysis for the specific surface area, total pore volume, and PSD of the ACF, ACF/CNF0, and ACF/CNF5 samples. The data in rows 1 and 2 for ACF and ACF/CNF0 show a decrease in the surface area, pore volume, and microporosity, as well as an increase in the mesoporosity of the sample, following the growth of CNF on ACF. Changes in these surface characteristics were more significant in the ACF/CNF5 sample for which the BET area was measured as approximately 232 m^2/g and the micropore contents as approximately 30%. These results are indicative of the growth of relatively denser and narrower pore-size CNFs on ACFs prepared with CTAB. We revisit this finding later when discussing the SEM images.

It is important to mention that micropores are not accessible to nitrogen molecules due to diffusion limitations. This results in an underestimation of the surface area and pore volume when measured using nitrogen as the probe molecule at 77 K. Such observations have also been reported elsewhere for surface characterization of microporous solids.[36,37] In these studies, the

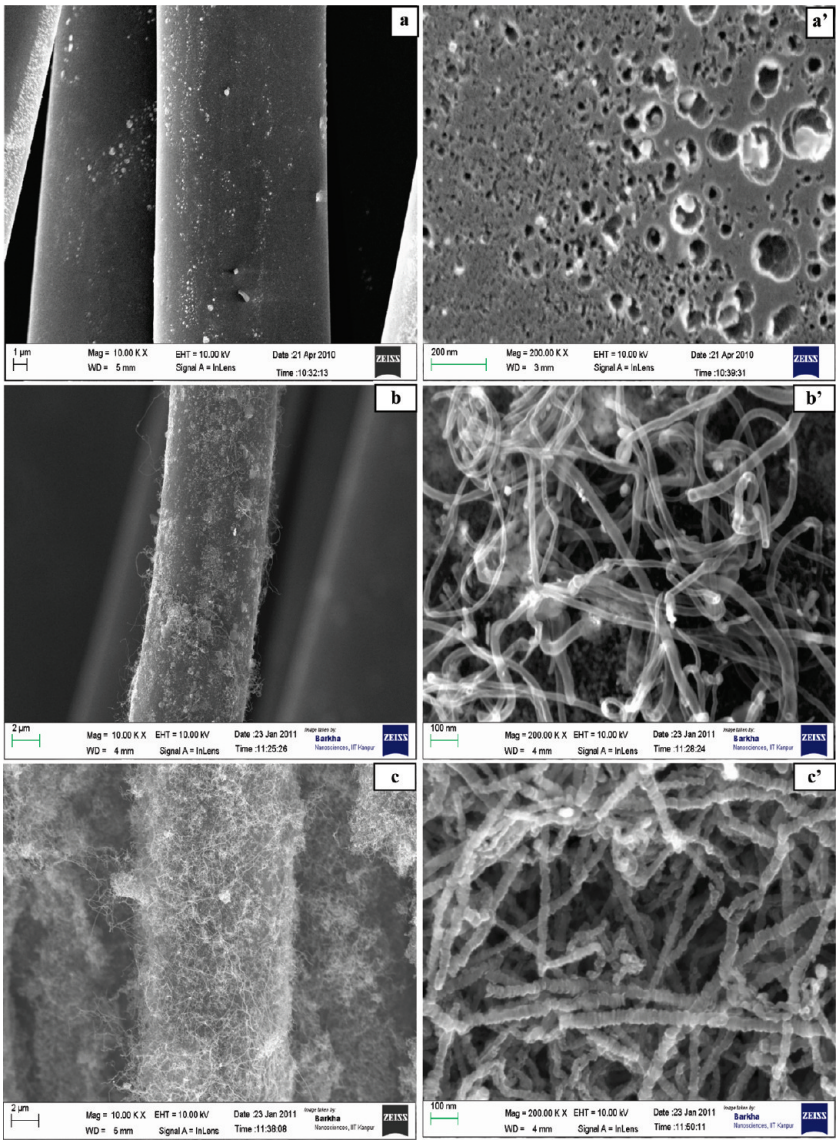

Figure 8. SEM images of (a, a′) ACF, (b, b′) ACF/CNF0, and (c, c′) ACF/CNF5.

underestimates, due to the use of nitrogen as the probe molecule, were as large as 45% for the surface area and total pore volume.

H_2-Chemisorption. Chemisorption analysis was carried out on the reduced samples (Ni-ACF) to determine the active metal surface area and the percentage of metal dispersion by the same Autosorb 1C Instrument used for the BET area measurements. Chemisorption was carried out using pure hydrogen gas as an adsorbate molecule. Approximately ∼0.1 g of the NiO-ACF sample was placed in a quartz sample cell. The sample was heated at a rate of 10 K min^{-1} to 473 K and degassed at the same temperature for 2 h under helium flow. Next, the temperature was increased at the same rate (10 K min^{-1}) to 673 K and treated with hydrogen at 10 cc per min for 2 h to convert all NiO into Ni. After hydrogen treatment, the sample was cooled to 60 °C under helium flow. The H_2-chemisorption test was subsequently carried out. The active metal surface area (per g of ACF/Ni) and Ni-dispersion (%) were calculated using the AS-Win software supplied with the instrument.

Table 3 presents the data of the H_2-chemisorption analysis. From the table, it is evident that the active Ni-surface area significantly increases (nearly 100%) for the Ni-ACF sample prepared with (5%) CTAB compared to the sample prepared without using CTAB. The active surface area and the metal dispersion were measured to be 0.713 m^2 g^{-1} and 2.67%, respectively, for the Ni-ACF sample prepared with 5% CTAB concentration.

These data corroborate the finding that CTAB enhances the amount of Ni transferred to ACF. Moreover, the higher is the nickel loading, the higher is the active metal surface area and percent metal dispersion. If the active nickel surface area is more, the yield of CNFs is also enhanced, as discussed in the following section.

Surface Morphology. Figure 8 displays the representative SEM images of different samples of ACFs and CNFs, grown with and without CTAB. The images are presented at small (10 KX) and large (200 KX) magnifications for each sample (ACF, ACF/CNF0, and ACF/CNF5). The corresponding scales shown on the images are in μm for low magnification and nm for high magnification.

As shown in Figure 8(a,a′), ACF presents a smooth surface with macropores visible on its external surface. Figure 8(b,b′)

dx.doi.org/10.1021/ie200741e |*Ind. Eng. Chem. Res.* 2012, 51, 2104–2112

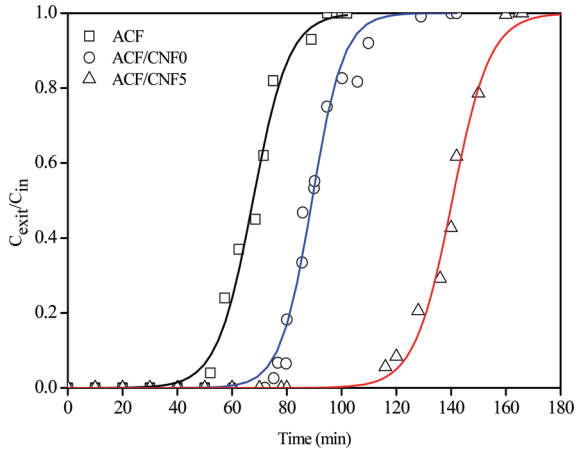

Figure 9. Breakthrough curves for the adsorption of 2-chloroethanol over different adsorbents (W = 1 g, Q_{N2} = 0.2 slpm, T = 40 °C).

displays the SEM images of the CNFs produced without using CTAB. The shiny Ni-particles at the tips of the fibers are suggestive of the growth of CNF by a tip-growth mechanism. The average diameter of the CNFs was measured to be in the range of 30−40 nm. However, the average diameter of the CNFs produced using 5% CTAB was in the range of 10−20 nm. Additionally, the growth of CNF was relatively more uniform and dense, as observed from the SEM images displayed in Figure 8(c,c′). Thus, it follows that the use of CTAB at the optimized concentration level (5%) during the impregnation step led to a more homogeneous distribution of much smaller NiO in ACF with minimal agglomeration. The size of the Ni-crystal produced following the reduction step was small, resulting in the growth of relatively denser and thinner CNFs. These results are consistent with the AAS, XRD, and H_2-chemisorption analysis.

Adsorption Study. *Breakthrough Analysis.* The adsorption of 2-chloroethanol was evaluated under flow (dynamic) conditions in a packed bed tubular adsorber. The details of the experimental setup have been published previously.[10] The setup consisted of an SS tube with perforations made on its peripheral surface. The tubular adsorber was contained within an SS-shell. The ACF or ACF/CNF fabrics were wrapped on the perforated section of the tube. Nitrogen gas laden with 2-chloroethanol flowed at a constant flow-rate into the adsorber. The treated gas flowed radially outward into the shell and exited from one end of the shell. The exit gas was analyzed for the solute concentration using a gas chromatograph (GC) (model: DS 5700, Nucon Co., India) equipped with a flame ionization detector (FID).

The adsorber containing the fresh sample was purged with nitrogen (100 cc per min) at 200 °C for 1 h. After the adsorber was cooled to 40 °C, the inlet connection to the adsorber was switched to N_2 gas (200 mL per min) saturated with 7600 ppm concentration of 2-chloroethanol. The gas was continuously passed through the adsorber until the packed bed was saturated with 2-chloroethanol.

Figure 9 describes the breakthrough curves of 2-chloroethanol on the ACF, ACF/CNF0, and ACF/CNF5 samples obtained under identical operating conditions. As shown, the breakthrough time (defined as the time when the exit gas concentration is 1% of the concentration at the inlet to the adsorber) was ∼42 min in the case of the ACF sample. The breakthrough time increased to ∼62 min for the ACF/CNF0 sample. A significant further increase

Table 4. Adsorptive Loading of 2-Chloroethanol on Different Metrics[a]

		loading		
sample	C_{CTAB} (%)	g/g of ACF	g/m^2 of ACF	(g/g-Ni)
ACF		0.321	0.0002	-
ACF/CNF0	0	0.520	0.0005	2.261
ACF/CNF5	5	0.758	0.0033	1.204

[a] Abbreviation: C_{CTAB} = concentration of CTAB.

(nearly twice) in the breakthrough time (∼110 min) was observed for the ACF/CNF5 sample. The data indicate the superior performance of the CNFs grown on ACFs in comparison to the substrate ACFs. More importantly, the significantly improved performance of the ACF/CNF composites prepared using CTAB can be observed from the figure. From the breakthrough curves, one can also observe an increase in the total saturation time (defined as the time when the exit gas concentration is within 99% of the concentration at the inlet to the absorber) from ∼80 min for the ACF sample to ∼100 min for the ACF/CNF0 sample and to ∼160 min for the ACF/CNF5 sample. These results show that CTAB considerably enhanced the growth of CNFs on ACFs via the increased loading of Ni-particles on ACFs during the impregnation step, which in turn increased the adsorption performance of ACF/CNF5. These performance characteristics of ACF/CNF5 are thus consistent with the surface structural characterizations described previously in the paper.

The adsorptive loading of the organic solute (w/w) on different samples was obtained from the total uptake of the solute by the adsorbent materials. The uptake was calculated by integrating along the breakthrough curve between the step change in the inlet concentration (incipience of the adsorption test) and the saturation time (the instance when the bed is saturated). The mathematical expression for calculating solute loading in a typical breakthrough experiment is as follows:

$$uptake\ (mg) = Q\left(C_{in}T - \int_0^T C_{exit}\ dt\right)$$

where T is the total time of adsorption when the bed is saturated with solute. C_{in} and C_{exit} are the inlet and the exit solute concentrations, respectively, and Q is the flow-rate of the gas. Table 4 summarizes the adsorptive loading of 2-chloroethanol on the adsorbents in different metrics (g/g-sample, g/m^2 of sample, g/g-Ni) calculated from the above-equation for the solute uptake. It is evident from the table that the loading of 2-chloroethanol was obtained as 0.758 g/g on ACF/CNF5, which is approximately 2.3 times that of the parent substrate, ACF, and ∼1.5 times of that obtained for the ACF/CN0 sample. Loading can also be expressed in other metrics, for example, 0.0033 g/m^2 based on the specific BET surface area and 1.204 g/g based on the Ni-loading for the ACF/CNF5 sample in comparison to 0.0005 g/m^2 and 2.261 g/g, respectively, for the ACF/CNF0 sample.

CONCLUSIONS

The introduction of CTAB during metal impregnation is an effective means of obtaining smaller monodispersed Ni-particles and in preserving their nonagglomerated identity in the impregnation step. This facilitated maximal transfer of Ni from the bulk

solution to the ACF surfaces. From the XRD spectra, the average size of Ni-particles in ACF, prepared using CTAB, is ~6 nm; much smaller than ~14 nm for the Ni-particle impregnated in the ACF, without using the surfactant. The surfactant modified ACF thus produces much denser and more uniform growth of CNFs during the CCVD step. The improved structural features of the CNFs grown with CTAB thus have a significantly improved adsorption capacity (0.758 g/g) for 2-chloroethanol, which is approximately 1.5 times that obtained on CNFs produced without using CTAB.

AUTHOR INFORMATION

Corresponding Authors

*(A.S.) Tel.: 91-512-2597026. E-mail: ashutos@iitk.ac.in. (N.V.) Tel.: 91-512-2596124. Fax: 91-512-2590104. E-mail: nishith@iitk.ac.in.

ACKNOWLEDGMENT

It is a special pleasure to be a part of the Festschrift for Professor K.D.P. Nigam. The authors acknowledge the support from DRDO, New Delhi, India in the form of a research grant, and DST, New Delhi, India through its Center on Nanosciences. The authors also acknowledge the supply of ACF from Kynol Inc., Tokyo (Japan).

REFERENCES

(1) Jia, R.; Huijuan, L.; Jiuhui, Q.; Aimin, W.; Ruihua, D. Characterization and adsorption behavior of a novel triolein-embedded activated carbon composite adsorbent. *Chin. Sci. Bull.* **2005**, *50* (23), 2788.

(2) Liu, H.; Qu, J.; Dai, R.; Ru, J.; Wang, Z. A biomimetic absorbent for removal of trace level persistent organic pollutants from water. *Environ. Pollut.* **2007**, *147*, 337.

(3) Ortiz, X.; Carabellido, L.; Marti, M; Martia, R; Tomas, X; Diaz-Ferrero, J. Elimination of persistent organic pollutants from fish oil with solid adsorbents. *Chemosphere* **2011**, *82*, 1301.

(4) Huang, L.; Yang, Z.; Li, B.; Hu, J.; Zhang, W.; Ying, W.-C. Granular activated carbon adsorption process for remove trichloroethlyle from ground water. *AIChE J.* **2010**, *57* (2), 542.

(5) Hajizadeh, Y.; Onwudili, J. A.; Williams, P. T. Removal potential of toxic 2378-substituted PCDD/F from incinerator flue gases by waste-derived activated carbons. *Waste Manage.* **2011**in press.

(6) Gaur, V.; Sharma, A.; Verma, N. Preparation and characterization of ACF for the adsorption of BTX and SO_2. *Chem. Eng. Process.* **2006a**, *45*, 1.

(7) Gaur, V.; Asthana, R.; Verma, N. (2006b). Removal of SO_2 by activated carbon fibers in the presence of O_2 and H_2O. *Carbon* **2006b**, *44*, 46.

(8) Moon, S.-H.; Shim, J.-W. A novel process for CO_2/CH_4 gas separation on activated carbon fibers-electric swing adsorption. *J. Colloid Interface Sci.* **2006**, *298*, 523.

(9) Yao, M.; Zhang, Q.; Hand, D. W.; Perram, D.; Taylor, R. Adsorption and regeneration on activated carbon fiber cloth for volatile organic compounds at indoor concentration levels. *J. Air Waste Manage. Assoc.* **2009**, *59* (1), 31.

(10) Bikshapathi, M.; Mandal, S.; Mathur, G. N.; Sharma, A.; Verma, N.; Modification of activated carbon fiber by metal dispersion and surface functionalization for the removal of 2-chloroethanol. *Ind. Eng. Chem. Res.*, published online January 14, 2011, http://pubs.ace.org/doi/10.1021/ie101860e.

(11) Gupta, A. K.; Deva, D.; Sharma, A.; Verma, N. Adsorptive removal of fluoride by micro-nanohierarchal web of activated carbon fibers. *Ind. Eng. Chem. Res.* **2009**, *48* (21), 9697.

(12) Gupta, A. K.; Deva, D.; Sharma, A.; Verma, N. Fe-grown carbon nanofibers for removal of arsenic (V) in wastewater. *Ind. Eng. Chem. Res.* **2010**, *49* (15), 7074.

(13) Rathore, R. S.; Srivastava, D. K.; Agarwal, A. K.; Verma, N. Development of surface-functionalized activated carbon fiber for control of NO and particulate matter. *J. Hazard. Mater.* **2010**, *173*, 211.

(14) Chakraborty, A.; Deva, D.; Sharma, A.; Verma, N. Adsorbents based on carbon microfibers and carbon nanofibers for the removal of phenol and lead from water. *J. Colloid Interface Sci.* **2011**, *359*, 228–239.

(15) Singhal, R. M.; Sharma, A.; Verma, N. Micro-nano-hierarchal web of activated carbon fibers for catalytic gas adsorption and reaction. *Ind. Eng. Chem. Res.* **2008**, *47*, 3700.

(16) Soukupov, J.; Kvıtek, L.; Panacek, A. Comprehensive study on surfactant role on silver nanoparticles (NPs) prepared via modified tollens process. *Mater. Chem. Phys.* **2008**, *111*, 77.

(17) Chen, D.-H.; Wu, S.-H. Synthesis of nickel nanoparticles in water-in-oil microemulsions. *Chem. Mater.* **2000**, *12*, 1354.

(18) Hou, Y.; Kondoh, H.; Ohta, T.; Gao, S. Size-controlled synthesis of nickel nanoparticles. *Appl. Surf. Sci.* **2005**, *241*, 218.

(19) Chen, D.-H.; Hsieh, C.-H. Synthesis of nickel nanoparticles in aqueous cationic surfactant solutions. *J. Mater. Chem.* **2002**, *12*, 2412.

(20) Zhang, D. E.; Ni, X. M.; Zheng, H. G.; Li, Y.; Zhang, X. J.; Yang, Z. P. Synthesis of needle-like nickel nanoparticles in water-in-oil microemulsion. *Mater. Lett.* **2005**, *59*, 2011.

(21) You-xian, Z.; Wen-jie, F.; Xue-qin, A. Preparation of nickel nanoparticles in emulsion. *Trans. Nonferrous Met. Soc. China* **2008**, *18*, 212.

(22) Santra, S.; Tapec, R.; Theodoropoulou, N.; Dobson, J.; Hebard, A.; Tan, W. Synthesis and characterization of silica-coated iron oxide nanoparticles in microemulsion: The effect of nonionic surfactants. *Langmuir* **2001**, *17* (10), 2900.

(23) Zheng, T.; Nishiyama, N.; Egashira, Y.; Ueyama, K. Ionic surfactant-mediated synthesis of Pt nanoparticles/nanoporous carbons composites. *Colloids and Surfaces A: Physicochem. Eng. Aspects* **2005**, *262*, 52.

(24) AL-Thabaiti, S. A.; Al-Nowaiser, F. M.; Obaid, A. Y.; Al-Youbi, A. O.; Khan, Z. Formation and characterization of surfactant stabilized silver nanoparticles: A kinetic study. *Colloids Surf., B* **2008**, *67*, 230.

(25) Farrukah, M. A.; Heng, B.-T.; Adnan, R. Surfactant-controlled aqueous synthesis of SnO_2 nanoparticles via the hydrothermal and conventional heating methods. *Turk. J. Chem.* **2010**, *34*, 537.

(26) Meng, L.-Y.; Moon, C.-W.; Im, S.-S.; Lee, K.-H.; Byun, J.-H.; Park, S.-J. Effect of Ni catalyst dispersion on the growth of carbon nanofibers onto carbon fibers. *Microporous Mesoporous Mater.* **2011**, *142*, 26–31.

(27) Vaisman, L.; Wagner, H. D.; Marom, G. The role of surfactants in dispersion of carbon nanotubes. *Adv. Coll. Inter. Sci.* **2006**, *128–130*, 37.

(28) Datsyuk, V.; Landois, P.; Fitremann, J.; Peigney, A.; Galibert, A. M.; Brigitte Soula, B.; Flahaut, E. Double-walled carbon nanotube dispersion via surfactant substitution. *J. Mater. Chem.* **2009**, *19* (18), 2729.

(29) Seelenmeyer, S.; Ballauff, M. Analysis of surfactants adsorbed onto the surface of latex particles by small-angle X-ray scattering. *Langmuir* **2000**, *16* (9), 4094.

(30) Singh, B. P.; Menchavez, R.; Takai, C.; Fuji, M.; Takahashi, M. Stability of dispersions of colloidal alumina particles in aqueous suspensions. *J. Colloid Interface Sci.* **2005**, *291*, 181.

(31) Lim, S.; Yoon, S.-H.; Shimizu, Y.; Jung, H.; Mochida, I. Surface control of activated carbon fiber by growth of carbon nanofiber. *Langmuir* **2004**, *20*, 5559.

(32) Tzeng, S.-S.; Hung, K.-H.; Ko, T.-H. Growth of carbon nanofibers on activated carbon fiber fabrics. *Carbon* **2006**, *44*, 859.

(33) Teo, K. B. K. Catalytic synthesis of carbon nanotubes and nanofibers. *Encyclopaedia of Nanosciences and Nanotechnology*; American Scientific: Stevenson Ranch, CA, 2003; Vol. X, p 1.

(34) Cuerda-Correa, E. M.; Macıas-Garcıa, A.; Dıez, M. A. D.; Ortiz, A. L. Textural and morphological study of activated carbon fibers prepared from kenaf. *Microporous Mesoporous Mater.* **2008**, *111*, 523.

(35) Lopez, B. M. C.; Martınez-Alonso, A.; Tascon, J. M. D. Microporous texture of activated carbon fibres prepared from Nomex aramid fibres. *Microporous Mesoporous Mater.* **2000**, *34*, 171.

(36) Danna, A. B. M.; Iyuke, S. E.; Fakhrul-Razi, A.; Chuah, T. G.; Atieh, M. A.; Al-Khatib, M. F. Synthesis and characterization of carbon nano-structures for methane storage. *Environmental Informatics Archives* **2003**, *1*, 597.

(37) Lozano-Castello, D.; Cazorla-Amoros, D.; Linares-Solano, A. Usefulness of CO_2 adsorption at 273 K for the characterization of porous carbons. *Carbon* **2004**, *42*, 1231.